

# Structural Evolution of Metastable Protein Aggregates in the Presence of Trivalent Salt Studied by (V)SANS and SAXS

Andrea Sauter,<sup>†</sup> Fajun Zhang,<sup>\*,†</sup> Noemi K. Szekely,<sup>‡</sup> Vitaliy Pipich,<sup>‡</sup> Michael Sztucki,<sup>§</sup> and Frank Schreiber<sup>†</sup>

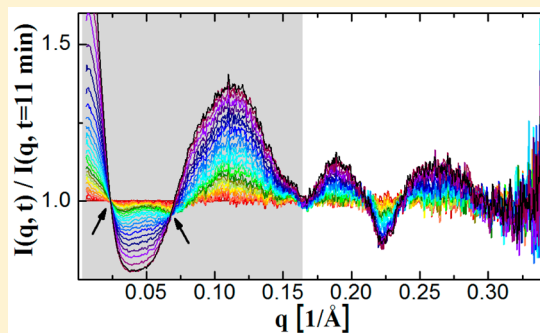
<sup>†</sup>Institut für Angewandte Physik, Universität Tübingen, Auf der Morgenstelle 10, 72076 Tübingen, Germany

<sup>‡</sup>Forschungszentrum Jülich GmbH, JCNS @ MLZ, Lichtenbergstraße 1, 85747 Garching, Germany

<sup>§</sup>European Synchrotron Radiation Facility, 71 avenue des Martyrs, 38043 Grenoble Cedex 9, France

## Supporting Information

**ABSTRACT:** We present a study of the structural evolution of protein aggregates formed in solutions of a globular protein,  $\beta$ -lactoglobulin (BLG), in the presence of  $YCl_3$ . These aggregates are often observed before crystallization starts and they are metastable with respect to the crystalline phase. Here we focus on the characterization of the hierarchical structure of this intermediate phase and its temperature dependent structure evolution using a combination of (very) small angle neutron and X-ray scattering (VSANS, SANS, and SAXS). Results show that the hierarchical structure ranges from nanometer scale protein monomer, dimer and compact protein clusters to micrometer scale fractal protein aggregates. Upon cooling, the overall hierarchical structure is preserved, but the evolution of the internal structure within the aggregates is clearly visible: the monomer–monomer correlation peak reduces its intensity and disappears completely at lower temperatures, whereas the cluster–cluster correlation is enhanced. At a larger length scale, the fractal dimension of protein aggregates increases. The kinetics of the structure change during a temperature ramp was further investigated using time-resolved SAXS. The time dependent SAXS profiles show clear isosbestic points and the kinetics of the structural evolution can be well described using a two-state model. These dynamic properties of protein aggregates on a broad length scale may be essential for being the precursors of nucleation.



## INTRODUCTION

Protein crystallization, as an important research field, provides not only the most successful way for determining high resolution structures of biomacromolecules but also rich conditions for exploring the early stage of crystallization. For example, it is very common to observe oil-like droplets (a protein rich liquid phase) in the crystallization assay before crystals appear. This liquid–liquid phase separation (LLPS) in protein solutions has been demonstrated to be metastable with respect to the crystalline phase, thus the coexistence line is located below the solubility line in a typical phase diagram.<sup>1–5</sup> In addition to LLPS, studies have also shown that the mesoscopic protein clusters may also play a crucial role in the nucleation process.<sup>6–10</sup> The existence of protein clusters or a metastable LLPS may change the kinetic pathway of crystal nucleation dramatically.

The pioneering work by ten Wolde and Frenkel showed that far from the metastable LLPS region nucleation follows the classical mechanism, i.e., nuclei form directly in a supersaturated solution with the same structure and density of the final crystalline phase.<sup>11–13</sup> However, when approaching the critical point, dense liquid-like droplets form first which further follow a structural change toward crystallization.<sup>14</sup> Further

theoretical studies and simulations also suggest that the existence of a metastable intermediate phase can promote crystal nucleation.<sup>14–16</sup> In the past decade, increasing evidence has shown that clusters, amorphous nanoparticles and other precursors may serve as an important intermediate for crystallization.<sup>9,17–21</sup> Thus, huge efforts have been made on characterizing the structure of these intermediate phases for a better understanding of their role in the crystal nucleation process.<sup>7–9,21–27</sup>

In our previous work, we found that multivalent metal ions provide an efficient way in tuning the effective protein–protein interactions in solution, leading to complex phase behavior including reentrant condensation (RC), LLPS, cluster formation and crystallization.<sup>28–34</sup> The rich phase behavior induced by the metal ions can be used to optimize conditions for growth of high quality protein single crystals, and to study the *pathways* of protein crystallization.<sup>35–37</sup> Figure 1 shows the experimental phase diagram of  $\beta$ -lactoglobulin (BLG) in the presence of  $YCl_3$ . We observe the so-called reentrant

Received: April 7, 2016

Revised: May 14, 2016

Published: June 10, 2016

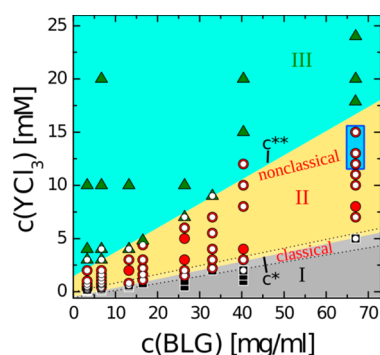


**Figure 1.** Experimental phase diagram of BLG in the presence of  $\text{YCl}_3$  determined at 21 °C. Regimes I (black squares), II (red circles), III (green triangles) correspond to clear, turbid, and clear states, respectively. Small white circles mark samples crystallized after 1 week at 4 °C. The blue rectangle marks sample conditions studied in this work. The label of *classical* indicates that near  $c^*$  crystallization takes place without visible precursor; the label of *nonclassical* indicates that close to  $c^{**}$  aggregates or a dense liquid phase appear before crystallization as reported in a previous study.<sup>28</sup>

condensation behavior, i.e. a phase separated state (regime II) exists in between two boundary salt concentrations  $c^* < c^{**}$ . Outside of regime II, the samples are clear. The physical mechanism of this RC behavior is due to the effective charge inversion of proteins and a cation mediated attraction.<sup>28,38</sup> Studies on the protein crystallization in different regions of Figure 1 have shown that, close to  $c^*$ , crystallization takes place without visible intermediates. Close to  $c^{**}$ , protein aggregates or dense liquid droplets form first. After an induction time, nucleation starts and crystal growth consumes the intermediate phase. In the end, only crystals are left.<sup>28,35</sup>

One of the interesting observations of the intermediate states is the morphology change with time: the amorphous protein aggregates develop into a network which further relaxes into a liquid-like state.<sup>28,35</sup> In fact, little is known about the internal structures of the intermediate and their development with time and temperature. We thus performed a systematic study on these metastable protein aggregates using (V)SANS and SAXS. In particular, we focus on the structural features at different length scales and the kinetics of the structural evolution with time and temperature.

## EXPERIMENTAL SECTION

**Materials.** The globular protein  $\beta$ -lactoglobulin (BLG) from bovine milk was purchased from Sigma-Aldrich (product no: L3908). This product is a mixture of the genetic variants A and B that differ at two positions in the primary sequence of 162 amino acids in total.<sup>39</sup> At room temperature and neutral pH, BLG is acidic (isoelectric point of 5.2) and predominantly in dimeric state.<sup>39,40</sup>  $\text{YCl}_3$  was also purchased from Sigma-Aldrich as an anhydrous powder with a purity of 99.99% (product no: 451363).

For sample preparation, appropriate amounts of salt stock solution, degassed Milli-Q (18.2 M $\Omega$ , Merck Millipore) water and protein stock solution were mixed. Stock solutions were prepared by dissolving the salt or protein powder in degassed Milli-Q water. No additional buffer was added. The protein concentration of stock solutions was determined by UV absorption measurements using an extinction coefficient of 0.96 l  $\times$  g<sup>-1</sup>  $\times$  cm<sup>-1</sup> at a wavelength of 278 nm.<sup>41</sup> The pH of the solutions was monitored using a Seven Easy pH instrument

from Mettler Toledo. The pH values under current experimental conditions were  $6.5 \pm 0.2$ , higher than the  $pI = 5.2$  of BLG.<sup>40</sup>

**Methods.** Fourier transform infrared spectroscopy (FTIR) (IFS 48 from Bruker) was applied to monitor the stability of the protein secondary structure under the experimental conditions as a function of temperature and salt concentration. Samples in the same composition but in heavy water ( $\text{D}_2\text{O}$ ) were prepared for a better signal-to-noise ratio.

Small angle X-ray scattering (SAXS) experiments were performed on beamline ID2 at the ESRF (Grenoble, France) using a sample-to-detector distance of 2 m. The beam energy was set to 16 keV, and the accessed  $q$  values ranged from 0.006 to 0.34  $\text{\AA}^{-1}$ . The data sets were reduced by subtracting the scattering of pure salt solution as a background. More detailed information on  $q$ -resolution calibration and data reduction can be found in refs 42 and 43. The samples were measured using a quartz glass capillary with a diameter of 2 mm. For the time-resolved measurements with a temperature ramp from 37 to 10 °C, the exposure time was 0.1 s, the waiting time between measurements was 300 s. The first SAXS data was collected about 11 min after sample preparation.

Small angle neutron scattering (SANS) was performed at KWS2 instrument operated by JCNS at the Heinz Maier-Leibnitz Zentrum (MLZ), Garching, Germany. The utilized neutron wavelength was 4.5  $\text{\AA}$  with  $\Delta\lambda/\lambda = 20\%$ . The sample-to-detector distances were 2, 8, and 20 m. The resulting total  $q$ -range was from  $2.2 \times 10^{-3}$  to 0.34  $\text{\AA}^{-1}$ .

Very small angle neutron scattering (VSANS) was performed at the instrument KWS3 instrument (operated by JCNS at the Heinz Maier-Leibnitz Zentrum (MLZ), Garching, Germany) with a sample-to-detector distance of 10 m. The applied neutron wavelength was 12.8  $\text{\AA}$  with  $\Delta\lambda/\lambda = 20\%$ , corresponding to a  $q$ -range from  $2.3 \times 10^{-4}$  to  $2.1 \times 10^{-3}$   $\text{\AA}^{-1}$ . (V)SANS data reduction and absolute intensity calibration was performed using the program QtiKWS provided by JCNS.<sup>44</sup>

**Data Analysis.** The scattering intensity of SANS experiments of protein solutions can be described as

$$I(q) = N_p(\Delta\rho)^2 V_p^2 P(q)S(q) + B_{inc} \quad (1)$$

where  $N_p$  is the number density of proteins per unit volume;  $V_p$  is the volume of a single protein;  $\Delta\rho$  is the difference in scattering length density between protein and the solvent;  $B_{inc}$  is the incoherent background;  $P(q)$  and  $S(q)$  are the form factor and the structure factor, respectively. The momentum transfer is defined as  $q = 4\pi/\lambda \sin \theta$  with the scattering angle  $2\theta$ . The size and shape of structures at different length scales, such as the native dimer and aggregates, are described using a spherical or ellipsoidal form factor. The effective interactions are described using structure factors calculated from different potentials that are listed in the following.

The hard sphere potential is defined by

$$U_{HS}(r) = \begin{cases} \infty & r \leq \sigma \\ 0 & r > \sigma \end{cases} \quad (2)$$

with the hard sphere diameter of  $\sigma$ . The effective hard sphere diameter is calculated by equating the second virial coefficient of the ellipsoid to a sphere having the same value.<sup>45,46</sup> The corresponding structure factor is obtained by solving the Ornstein–Zernike (OZ) equation numerically with the Percus–Yevick (PY) closure.<sup>47</sup>

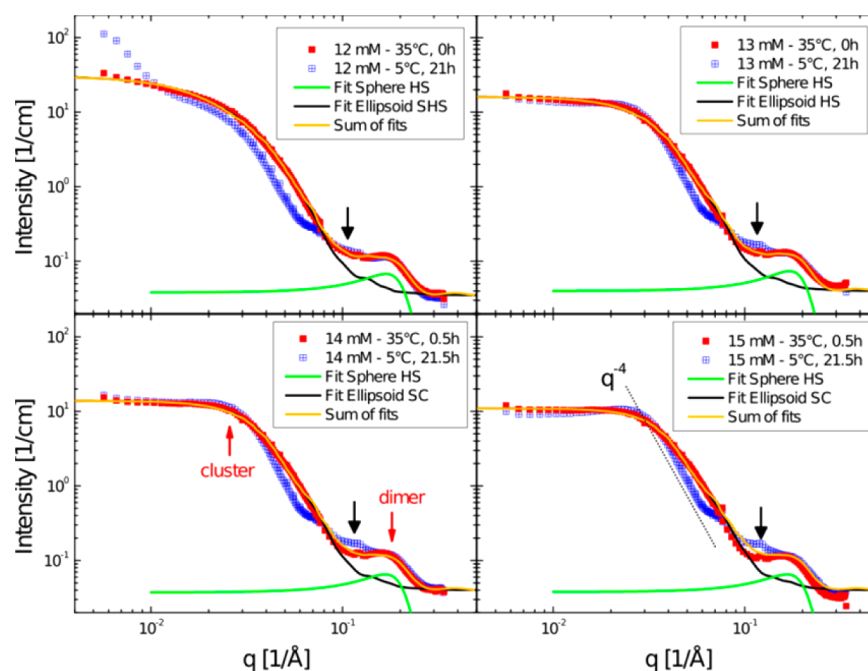


**Figure 2.** Structure and interactions of protein-salt mixtures characterized by SANS in dependence of temperature and salt concentration. Scattering contributions from protein clusters and dimers were analyzed using a sum model. Model descriptions for different  $q$  ranges were shown in lines and discussed in detail in the main text. The protein concentration of the samples was fixed to 67 mg/mL, the salt concentrations were 12, 13, 14, and 15 mM  $\text{YCl}_3$ . Data presented were collected at 35 and 5 °C, respectively. The times given in the legend were the starting times and each measurement took about 2.5 h. The black arrows indicates an additional structural change that becomes more pronounced with increasing salt concentration.

The sticky hard sphere potential is used to describe the short-range attraction between protein clusters, which is defined by<sup>48</sup>

$$U_{SHS}(r) = \begin{cases} \infty & r \leq \sigma \\ -u_0 = \ln\left(\frac{12\tau\Delta}{\sigma + \Delta}\right) & \sigma < r < \sigma + \Delta \\ 0 & r > \sigma + \Delta \end{cases} \quad (3)$$

where  $\tau$  is the stickiness parameter and usually the limit  $\Delta \rightarrow 0$  is taken.

The screened Coulomb potential is used to describe the long-range electrostatic repulsion of protein clusters due to the accumulated charges, which is defined by

$$U_{SC}(r) = \begin{cases} \frac{Z^2 e^2}{\epsilon(1 + \kappa_D \sigma/2)^2} \frac{\exp[-\kappa_D(r - \sigma)]}{r} & r > \sigma \\ \infty & r \leq \sigma \end{cases} \quad (4)$$

with  $Z$  the protein surface charge,  $e$  the electronic charge, and  $\epsilon$  the dielectric constant of the solvent.  $\kappa_D$  is the inverse of the Debye screening length, determined by the ionic strength of the solution.

The corresponding structure factors for both the sticky hard sphere potential and the screened Coulomb potential were calculated by solving the OZ equation using the mean-spherical approximation closure relation.<sup>48–50</sup> Data fitting was performed using ORIGINPRO (two-state analysis) and IGOR PRO with macros provided by NIST.<sup>46</sup>

## RESULTS AND DISCUSSION

**Structures and Interactions in Protein Solutions Studied by SANS.** We first present an overview of interactions and structures in protein solutions as a function of salt concentration and temperature. In order to study the structural evolution as a function of temperature (observable range 0–40 °C), we chose samples with a fixed BLG concentration of 67 mg/mL and  $\text{YCl}_3$  concentrations between 12 and 15 mM. According to Figure 1, these samples at room temperature are in the upper area of regime II as labeled by the blue rectangle. When prepared at 35 °C, the samples with 13–15 mM salt were clear (regime III), only the sample with 12 mM salt was turbid. When cooled down to 5–10 °C, all samples became turbid (regime II) in consistence with Figure 1.

Figure 2 presents the SANS results for these samples at 35 and 5 °C. Measurements at temperatures in between are shown in the Supporting Information (Figure S1). At 35 °C, the SANS curves for all samples are similar in the high  $q$  region, but the intensity at the low  $q$  region decreases with increasing salt concentration. For the sample with 12 mM salt, the low  $q$  upturn is consistent with the observation that this sample is already turbid at 35 °C, which becomes more significant at 5 °C. The other samples do not have such a strong intensity increase at the low  $q$  region even after 21 h at 5 °C.

To understand the structural features of the protein aggregates at different length scales, a global fit with a unified model would be desirable. Unfortunately, such a global fit is not feasible, in particular, if the structures at different length scales and their interactions vary from one to another. We thus apply several models in the following to analyze the structures and interactions for objects at different length scales and explain for each case the main information obtained.

The SANS curves in Figure 2 show two main steps in the intensity profiles at 0.03 and 0.18  $\text{\AA}^{-1}$ , which can be explained

by the contribution of small protein clusters and the native dimer of BLG, respectively. This observation is consistent with our previous measurements on this system using SAXS.<sup>51</sup> The dimer contribution has developed a visible dimer–dimer correlation peak. It was further analyzed using a simple spherical form factor and a hard-sphere potential. The radius of the spherical form factor is about 15 Å and was fixed for further data fitting. The volume fraction is between 0.26 and 0.27 and slightly decreases with increasing salt concentrations. The detailed fitting results are shown in the Supporting Information (Table S1).

For the cluster contribution in the low  $q$  region (below  $0.03 \text{ \AA}^{-1}$  in Figure 2), the scattering intensity decreases with increasing salt concentration. A correlation peak appears which becomes even stronger at lower temperature. With 14 and 15 mM  $\text{YCl}_3$ , a cluster–cluster correlation peak becomes visible at  $0.03 \text{ \AA}^{-1}$ , which corresponds to a center-to-center distance about 210 Å between clusters. Scattering intensities in the  $q$  range between 0.04 and  $0.07 \text{ \AA}^{-1}$  decrease linearly with slopes between  $-3.5$  (at  $35 \text{ }^\circ\text{C}$ ) and  $-4$  (at  $5 \text{ }^\circ\text{C}$ ). This behavior satisfies Porod's law and implies that the scatterers (protein clusters) at this length scale have a compact, nonfractal structure with a sharp interface. A model fit of the curves for 14 and 15 mM  $\text{YCl}_3$  using a screened Coulomb potential together with an ellipsoid form factor shows that the overall net charge increases with increasing salt concentration. While the charges are nearly constant with decreasing temperature, the effective size of the ellipsoid form factor and the volume fraction increase (Table S1). With 13 and 12 mM  $\text{YCl}_3$ , the data are better described using the hard-sphere and sticky hard-sphere potential, respectively, indicating that the effective interactions between the protein clusters undergo a transition from repulsive to attractive upon lowering the salt concentration. These rather compact protein clusters might be formed by the balance between the bridging effect of metal ions and the electrostatic repulsion due to the accumulated net charges.

Upon cooling from 35 to  $5 \text{ }^\circ\text{C}$ , the dimer and cluster contributions remain without visible changes. However, two more steps in the SANS profiles become visible at  $0.07$ – $0.08$  and  $0.12 \text{ \AA}^{-1}$  in Figure 2 for all samples. These new features correspond to structures of  $D = 2\pi/q \approx 90$ – $78$  and  $52 \text{ \AA}$ , respectively. The new structure at  $0.12 \text{ \AA}^{-1}$  (labeled using a black arrow) is more pronounced at higher salt concentrations. The formation of these hierarchical structures also suggests that proteins within the clusters have a certain flexibility for rearrangement upon cooling. It is interesting to see that the structure at  $0.07 \text{ \AA}^{-1}$  also exist in a thermal denatured whey protein (mainly BLG) microgel.<sup>52,53</sup> SAXS measurements of the microgel reveal not only a hierarchical and fractal structure but also a pronounced structural feature at  $0.07 \text{ \AA}^{-1}$ , which has been explained by the close neighbor effect or the internal organization of the denatured whey protein monomers within the microgel.<sup>52,53</sup> In our system, the proteins are certainly not denatured (see below). The appearance of the new structure feature reflects the flexibility and self-organization property of proteins under the current experimental conditions.

**Hierarchical Structure Characterized by (V)SANS and SAXS.** The hierarchical structure of the protein aggregates in samples with 67 mg/mL BLG and 15 mM  $\text{YCl}_3$  were further characterized using VSANS and SAXS to cover a broader  $q$ -range. As presented in Figure 3, the combined (V)SANS and SAXS data at 35 and  $5 \text{ }^\circ\text{C}$  provide the structure information from monomer–monomer correlation, and compact clusters

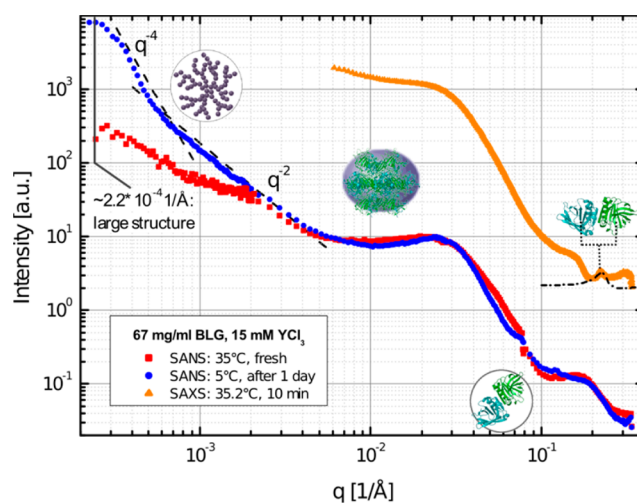


**Figure 3.** Hierarchical structure of protein aggregates characterized by (V)SANS and SAXS for a sample with 67 mg/mL BLG and 15 mM  $\text{YCl}_3$  at 35 and  $5 \text{ }^\circ\text{C}$ . The merged SANS data were obtained from KWS-3 (VSANS) and KWS-2 (SANS). SAXS data of the same sample at  $35 \text{ }^\circ\text{C}$  show an additional monomer–monomer correlation at  $q = 0.22 \text{ \AA}^{-1}$ . The structural interpretation at different length scales is also shown.

up to fractal aggregates in length scales from nanometer to micrometer. These structures at different length scales are illustrated with the assembled structures of protein (schematics) in Figure 3 and explained below.

First, the extended VSANS data in the low  $q$  region (below  $2 \times 10^{-3} \text{ \AA}^{-1}$ ) clearly show an increase in intensity at both temperatures. The asymptotically linear increase in intensity at lower  $q$  suggests larger protein aggregates that are more fractal than the clusters at smaller length scale. The fractal dimension,  $d$ , can be determined from the slopes of the VSANS curves in the  $q$  range between  $0.5 \times 10^{-3}$  and  $4 \times 10^{-3} \text{ \AA}^{-1}$ . The obtained values are around 1.7 and 1.9 before and after cooling, respectively. At even lower  $q$ , after cooling, another Porod region becomes visible and a plateau at around  $2 \times 10^{-4} \text{ \AA}^{-1}$  is visible, which indicates that the fractal aggregates can further organize into an even larger and more compact structure with a mean size of  $D = 2\pi/q \approx 3 \text{ }\mu\text{m}$ .

Second, SAXS data show additional structural features due to the higher resolution in the high  $q$  region. A peak at  $0.22 \text{ \AA}^{-1}$  is clearly visible in the SAXS curve (not visible in SANS) after preparation at  $35 \text{ }^\circ\text{C}$ , which can be attributed to the monomer–monomer correlation within clusters as discussed in our previous work.<sup>51</sup> The absence of the monomer–monomer correlation peak in SANS curves in Figure 2 may be due to the smearing effect of neutrons at high  $q$  with  $\Delta\lambda/\lambda = 20\%$ . Compared to the SAXS data, the overall SANS data are shifted toward higher  $q$  which causes the dimer shoulder in SANS to nearly overlap with the monomer–monomer correlation peak in SAXS. The shift of SANS data towards higher  $q$  is mainly due to the absent contribution of the hydrated water molecules around proteins, to which SAXS is more sensitive.<sup>54</sup>

We emphasize that the observed protein condensation is not caused by a change of the protein structure induced by  $\text{YCl}_3$  and further treatments. Figure 4 shows FTIR spectra for a sample with a BLG concentration of 67 mg/mL and 15 mM  $\text{YCl}_3$  under similar conditions as the SANS measurements (measurements for 12–14 mM can be found in the Supporting

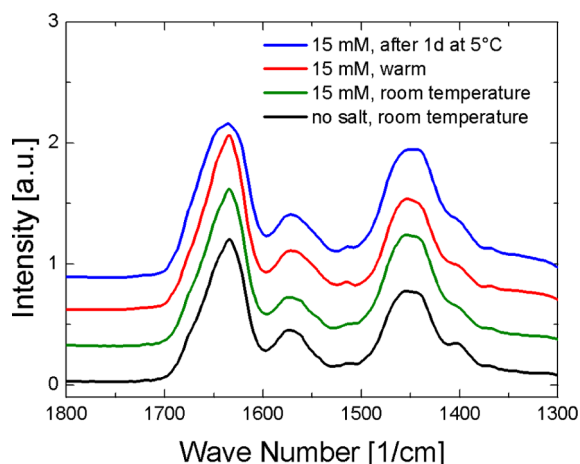


**Figure 4.** FTIR spectra collected at room temperature for protein samples with 67 mg/mL BLG and 15 mM  $\text{YCl}_3$  after different thermal treatments: (black) control measurement, sample without added salt; (green) sample prepared at room temperature; (red) sample prepared and equilibration at 35–38 °C for 1 h; (blue) sample prepared at 35 °C, then quenched and stored at 5 °C for a day. No visible changes on the secondary structure of the protein could be observed. Spectra were shifted in intensity for better visibility.

Information, Figure S2). For comparison, the spectrum of a protein solution with the same protein concentration but without added salt is also shown. As one can see, in all cases, the amide I and amide II bands are in the same shape and ratio of intensity. These measurements confirm that there is no significant change on the secondary structure of protein neither caused by addition of  $\text{YCl}_3$  nor by temperature change. We have also studied the stability of protein secondary structure in the presence of multivalent salts in  $\text{H}_2\text{O}$  and  $\text{D}_2\text{O}$  using circular dichroism (CD) and FTIR.<sup>30,43</sup> The consistency of the different techniques suggests that replacing  $\text{H}_2\text{O}$  by  $\text{D}_2\text{O}$  has no significant effects on the secondary structure of the protein. Moreover, the successful growth of high-quality crystals and fine structural analysis confirm that the proteins are still in their native state.<sup>28,35</sup>

**Structural Evolution Followed by Time-Resolved SAXS.** Previous studies using optical microscopy indicate that the protein aggregates formed after sample preparation can further relax into a liquid-like network within hours.<sup>35</sup> Later, crystallization occurs mainly at its interface. The hierarchical structure at different temperatures presented in the previous section indicates that the local structures change with time and temperature. In the following, the real-time SAXS data are analyzed in order to understand the transition kinetics.

The time-resolved SAXS data during a temperature ramp from 37 to 10 °C are presented in Figure 5a. In general, during the temperature ramp, the overall scattering profile is preserved, which is consistent with the SANS measurements in Figure 2. However, changes of the local structures are clearly visible. For example, the intensity at  $q$  ranges below 0.025  $\text{\AA}^{-1}$  increases with time (or decreasing temperature), whereas the intensity decreases with time in the  $q$  range between 0.025 and 0.075  $\text{\AA}^{-1}$ , resulting in an isosbestic point. Furthermore, the monomer–monomer correlation peak reduces with time and finally disappears. These changes are better presented in Figure 5b, where the SAXS data were divided by the first curve (about 11 min after sample preparation). This plot therefore displays the changes in this process.

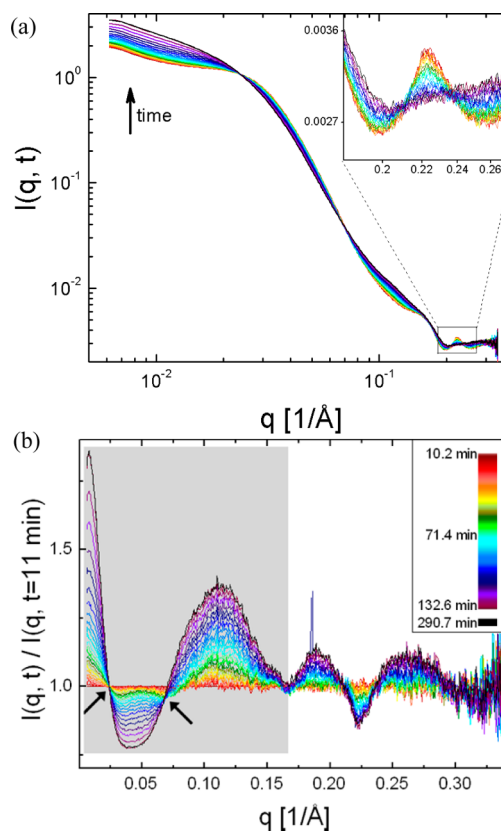


**Figure 5.** (a) Time-resolved SAXS profiles for a sample containing 67 mg/mL BLG with 15 mM  $\text{YCl}_3$  during a temperature ramp from 37 to 10 °C. The inset shows the zoom-in of the monomer–monomer correlation peak. (b) Modified SAXS curves from part (a) divided by the first curve.

The isosbestic (or iso-scattering) points at 0.025 and 0.075  $\text{\AA}^{-1}$  indicate that the system transforms from one state to the other and the scattering intensity for both states stays constant. Therefore, the scattering curves can be described as the sum of two constituents:<sup>55</sup>

$$I(q) = F(t)I_{\text{start}}(q) + [1 - F(t)]I_{\text{final}}(q) \quad (5)$$

$$F(t) = (I - I_{\text{final}}) / (I_{\text{start}} - I_{\text{final}}) \quad (6)$$

A two-state analysis was performed using eq 5 to fit the time-resolved SAXS data.  $I_{\text{start}}(q)$  is the first curve in time and  $I_{\text{final}}(q)$  the last one.  $F(t)$  describes the variation of the scattering intensity.

The obtained  $F(t)$  and  $1 - F(t)$  are plotted in Figure 6a, left. All SAXS curves can be modeled with a high precision. An example is presented in the right part of Figure 6a for the curve at 102 min. This analysis demonstrates that the internal structural evolution within the metastable protein aggregates proceeds via a simple two-state process.

The time and temperature dependency of the monomer–monomer correlation peak at 0.22  $\text{\AA}^{-1}$  was further analyzed by plotting the peak area as a function of time (or temperature) (see Figure 6b). The value of the area (also the shape of the correlation peak) is nearly constant before it starts to decrease at approximately 22 °C. Below ca. 13 °C (after 70 min), this correlation peak disappears completely. The crystallographic analysis in our previous work<sup>28</sup> indicates that the BLG dimer is the building block of the crystal lattice. Therefore, the

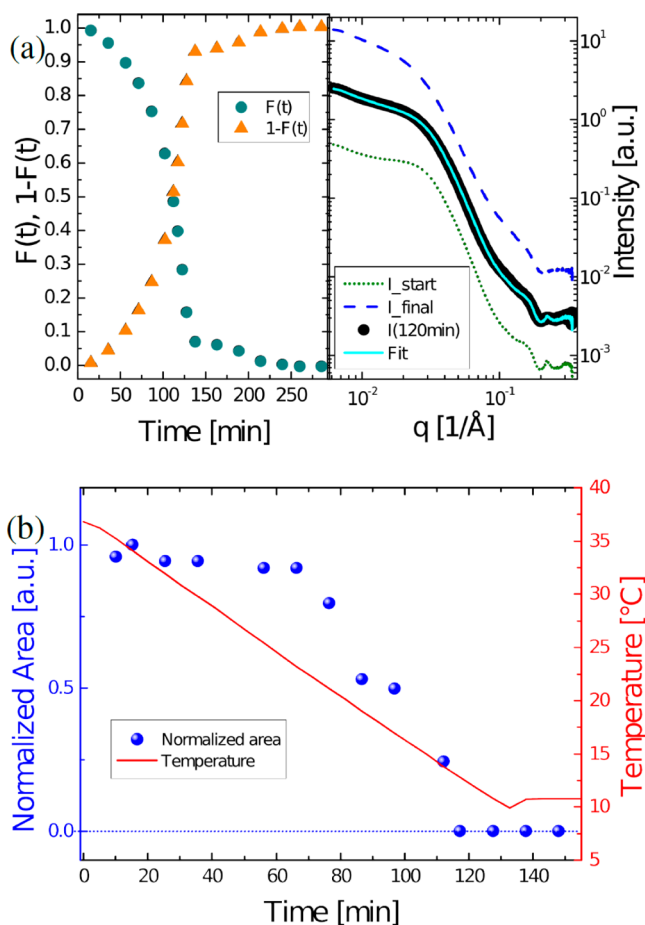


**Figure 6.** Further analysis of time-resolved SAXS data. (a) Two-state analysis of the structural evolution kinetics using eq 5. Left: plots of  $F(t)$  and  $1 - F(t)$  as a function of time. Right: example SAXS curve at 102 min after sample preparation (black) with obtained fit (cyan) along with the initial and final curve (shifted up and down for better visibility). (b) Plot of the area of the monomer–monomer correlation peak (blue data points) as a function of time. The area was determined by fitting the correlation peak with a Gaussian. The red solid line describes the temperature change with time.

temperature dependent monomer–monomer correlation peak may be related to the flexibility of proteins within the aggregates. Upon cooling or entering the crystal lattice, this flexibility is reduced. Note that in our previous work,<sup>51</sup> a similar sample has been measured using SAXS and Bragg peaks were observed after two cycles of a temperature ramp from 25 to 10 °C. The SAXS profiles in the present study are very similar, but no crystals are observed after the measurements. The exact reasons are unknown, but the different thermal history may be one of them.

## CONCLUSIONS

A hierarchy of structures of protein aggregates in aqueous solution of BLG and  $\text{YCl}_3$  which may serve as the intermediate for protein crystallization has been characterized using (V)SANS and SAXS. Structural features at different length scales ranging from monomer–monomer correlation in nanometers, the scattering of dimers, compact clusters, to a fractal structure in micrometer length scales have been identified.

When prepared at 35 °C, the monomer–monomer correlation is visible in the SAXS curves. After cooling to 5–10 °C, the dimer acts as an elementary building block and the monomer–monomer correlation peak disappears. The appearance of the monomer–monomer correlation reflects the flexibility of proteins within the aggregates. A cluster–cluster correlation peak becomes visible with increasing salt concentration. These rather compact protein clusters might be formed by the balance between the bridging effect of metal ions and the electrostatic repulsion due to the accumulated net charges. The appearance of the isosbestic points in the time-resolved SAXS data can be well described using a two-state model, indicating that the internal structure changes within the metastable protein aggregates follow a two-state process.

To be able to serve as the intermediate phase for crystal nucleation, the structure and the internal dynamics of these protein aggregates are crucial. While the structures at length scales larger than 1  $\mu\text{m}$  may be not directly related to the nucleation process, protein clusters of a few hundreds of Ångströms may. Together with the unique dynamic feature of the internal structures, i.e., the coupled, two-state feature of the internal structures (monomer and dimer), crystal nucleation within the metastable protein aggregates becomes possible. This observation is also consistent with our previous study of the crystal structures that the BLG dimer is the building block of the crystal lattice.<sup>28</sup>

## ASSOCIATED CONTENT

### Supporting Information

The Supporting Information is available free of charge on the ACS Publications website at DOI: 10.1021/acs.jpcb.6b03559.

SANS data fitting details; Table S1, list of fitting parameters; Figure S1, complete set of SANS data for Figure 2 in the main text; Figure S2, FTIR measurements for samples with 12, 13, 14, and 15 mM  $\text{YCl}_3$  (PDF)

## AUTHOR INFORMATION

### Corresponding Author

\*(F.Z.) E-mail: fajun.zhang@uni-tuebingen.de. Telephone: +49 (0)7071 2978670. Fax: +49 (0)7071 295110.

### Notes

The authors declare no competing financial interest.

## ACKNOWLEDGMENTS

We gratefully acknowledge funding from DFG and Landesgraduiertenförderung, as well as allocation of beamtime from ESRF and Forschungszentrum Jülich/FRM2 (Munich). We thank Dr. F. Roosen-Runge for valuable discussions. The authors gratefully acknowledge inspiring discussions with Dr. P. Fenter (Argonne National Laboratory). The authors gratefully acknowledge the financial support provided by JCNS to perform the neutron scattering measurements at the Heinz Maier-Leibnitz Zentrum (MLZ), Garching, Germany.

## REFERENCES

- (1) Delaye, M.; Clark, J.; Benedek, G. Coexistence Curves for Phase Separation in the Calf Lens Cytoplasm. *Biochem. Biophys. Res. Commun.* **1981**, *100*, 908–914.
- (2) Broide, M. L.; Berland, C. R.; Pande, J.; Ogun, O. O.; Benedek, G. B. Binary-Liquid Phase Separation of Lens Protein Solutions. *Proc. Natl. Acad. Sci. U. S. A.* **1991**, *88*, 5660–5664.

- (3) Muschol, M.; Rosenberger, F. Liquid–Liquid Phase Separation in Supersaturated Lysozyme Solutions and Associated Precipitate Formation/Crystallization. *J. Chem. Phys.* **1997**, *107*, 1953–1962.
- (4) Galkin, O.; Vekilov, P. G. Control of Protein Crystal Nucleation around the Metastable Liquid–Liquid Phase Boundary. *Proc. Natl. Acad. Sci. U. S. A.* **2000**, *97*, 6277–6281.
- (5) Wang, Y.; Lomakin, A.; Latypov, R. F.; Benedek, G. B. Phase Separation in Solutions of Monoclonal Antibodies and the Effect of Human Serum Albumin. *Proc. Natl. Acad. Sci. U. S. A.* **2011**, *108*, 16606–16611.
- (6) Li, Y.; Lubchenko, V.; Vekilov, P. G. The Use of Dynamic Light Scattering and Brownian Microscopy to Characterize Protein Aggregation. *Rev. Sci. Instrum.* **2011**, *82*, 053106.
- (7) Pan, W.; Galkin, O.; Filobelo, L.; Nagel, R. L.; Vekilov, P. G. Metastable Mesoscopic Clusters in Solutions of Sick-Cell Hemoglobin. *Biophys. J.* **2007**, *92*, 267–277.
- (8) Sleutel, M.; van Driessche, A. E. S. Role of Clusters in Nonclassical Nucleation and Growth of Protein Crystals. *Proc. Natl. Acad. Sci. U. S. A.* **2014**, *111*, E546–E553.
- (9) Gliko, O.; Neumaier, N.; Pan, W.; Haase, I.; Fischer, M.; Bacher, A.; Weinkauff, S.; Vekilov, P. G. A Metastable Prerequisite for the Growth of Lumazine Synthase Crystals. *J. Am. Chem. Soc.* **2005**, *127*, 3433–3438.
- (10) Stradner, A.; Sedgwick, H.; Cardinaux, F.; Poon, W. C. K.; Egelhaaf, S. U.; Schurtenberger, P. Equilibrium Cluster Formation in Concentrated Protein Solutions and Colloids. *Nature* **2004**, *432*, 492–495.
- (11) Gebauer, D.; Cölfen, H. Prenucleation Clusters and Non-Classical Nucleation. *Nano Today* **2011**, *6*, 564–584.
- (12) Anderson, V. J.; Lekkerkerker, H. N. W. Insights into Phase Transition Kinetics from Colloid Science. *Nature* **2002**, *416*, 811–815.
- (13) Sear, R. Nucleation at Contact Lines where Fluid–Fluid Interfaces Meet Solid Surfaces. *J. Phys.: Condens. Matter* **2007**, *19*, 466106.
- (14) ten Wolde, P. R.; Frenkel, D. Enhancement of Protein Crystal Nucleation by Critical Density Fluctuations. *Science* **1997**, *277*, 1975–1978.
- (15) Hutchens, S. B.; Wang, Z.-G. Metastable Cluster Intermediates in the Condensation of Charged Macromolecule Solutions. *J. Chem. Phys.* **2007**, *127*, 084912.
- (16) Tóth, G. I.; Pusztai, T.; Tegze, G.; Tóth, G.; Gránásy, L. Amorphous Nucleation Precursor in Highly Nonequilibrium Fluids. *Phys. Rev. Lett.* **2011**, *107*, 175702.
- (17) Navrotsky, A. Energetic Clues to Pathways to Biomineralization: Precursors, Clusters, and Nanoparticles. *Proc. Natl. Acad. Sci. U. S. A.* **2004**, *101*, 12096–12101.
- (18) Banfield, J. F.; Welch, S. A.; Zhang, H.; Ebert, T. T.; Penn, R. L. Aggregation-Based Crystal Growth and Microstructure Development in Natural Iron Oxyhydroxide Biomineralization Products. *Science* **2000**, *289*, 751–754.
- (19) Furrer, G.; Phillips, B. L.; Ulrich, K.-U.; Pöthig, R.; Casey, W. H. The Origin of Aluminum Floccs in Polluted Streams. *Science* **2002**, *297*, 2245–2247.
- (20) Mintova, S.; Olson, N. H.; Valtchev, V.; Bein, T. Mechanism of Zeolite A Nanocrystal Growth from Colloids at Room Temperature. *Science* **1999**, *283*, 958–960.
- (21) Gliko, O.; Pan, W.; Katsonis, P.; Neumaier, N.; Galkin, O.; Weinkauff, S.; Vekilov, P. G. Metastable Liquid Clusters in Super- and Undersaturated Protein Solutions. *J. Phys. Chem. B* **2007**, *111*, 3106–3114.
- (22) Pan, W.; Vekilov, P. G.; Lubchenko, V. Origin of Anomalous Mesoscopic Phases in Protein Solutions. *J. Phys. Chem. B* **2010**, *114*, 7620–7630.
- (23) Chen, Q.; Vekilov, P. G.; Nagel, R. L.; Hirsch, R. E. Liquid–Liquid Phase Separation in Hemoglobins: Distinct Aggregation Mechanisms of the  $\beta 6$  Mutants. *Biophys. J.* **2004**, *86*, 1702–1712.
- (24) Liu, Y.; Wang, X.; Ching, C. B. Toward Further Understanding of Lysozyme Crystallization: Phase Diagram, Protein–Protein Interaction, Nucleation Kinetics, and Growth Kinetics. *Cryst. Growth Des.* **2010**, *10*, 548–558.
- (25) Sear, R. P. Nucleation via an Unstable Intermediate Phase. *J. Chem. Phys.* **2009**, *131*, 074702.
- (26) Zhang, T. H.; Liu, X. Y. How Does a Transient Amorphous Precursor Template Crystallization. *J. Am. Chem. Soc.* **2007**, *129*, 13520–13526.
- (27) Savage, J. R.; Dinsmore, A. D. Experimental Evidence for Two-Step Nucleation in Colloidal Crystallization. *Phys. Rev. Lett.* **2009**, *102*, 198302.
- (28) Zhang, F.; Zocher, G.; Sauter, A.; Stehle, T.; Schreiber, F. Novel Approach to Controlled Protein Crystallization through Ligandation of Yttrium Cations. *J. Appl. Crystallogr.* **2011**, *44*, 755–762.
- (29) Zhang, F.; Skoda, M. W. A.; Jacobs, R. M. J.; Zorn, S.; Martin, R. A.; Martin, C. M.; Clark, G. F.; Weggler, S.; Hildebrandt, A.; Kohlbacher, O.; et al. Reentrant Condensation of Proteins in Solution Induced by Multivalent Counterions. *Phys. Rev. Lett.* **2008**, *101*, 148101.
- (30) Zhang, F.; Weggler, S.; Ziller, M. J.; Ianeselli, L.; Heck, B. S.; Hildebrandt, A.; Kohlbacher, O.; Skoda, M. W. A.; Jacobs, R. M. J.; Schreiber, F. Universality of Protein Reentrant Condensation in Solution Induced by Multivalent Metal Ions. *Proteins: Struct., Funct., Genet.* **2010**, *78*, 3450–3457.
- (31) Zhang, F.; Roth, R.; Wolf, M.; Roosen-Runge, F.; Skoda, M. W. A.; Jacobs, R. M. J.; Stzucki, M.; Schreiber, F. Charge-Controlled Metastable Liquid–Liquid Phase Separation in Protein Solutions as a Universal Pathway Towards Crystallization. *Soft Matter* **2012**, *8*, 1313–1316.
- (32) Zhang, F.; Roosen-Runge, F.; Sauter, A.; Wolf, M.; Jacobs, R. M. J.; Schreiber, F. Reentrant Condensation, Liquid–Liquid Phase Separation and Crystallization in Protein Solutions Induced by Multivalent Metal Ions. *Pure Appl. Chem.* **2014**, *86*, 191–202.
- (33) Roosen-Runge, F.; Heck, B. S.; Zhang, F.; Kohlbacher, O.; Schreiber, F. Interplay of pH and Binding of Multivalent Metal Ions: Charge Inversion and Reentrant Condensation in Protein Solutions. *J. Phys. Chem. B* **2013**, *117*, 5777–5787.
- (34) Soraruf, D.; Roosen-Runge, F.; Grimaldo, M.; Zanini, F.; Schweins, R.; Seydel, T.; Zhang, F.; Roth, R.; Oettel, M.; Schreiber, F. Protein Cluster Formation in Aqueous Solution in the Presence of Multivalent Metal Ions - a Light Scattering Study. *Soft Matter* **2014**, *10*, 894–902.
- (35) Sauter, A.; Oelker, M.; Zocher, G.; Zhang, F.; Stehle, T.; Schreiber, F. Nonclassical Pathways of Protein Crystallization in the Presence of Multivalent Metal Ions. *Cryst. Growth Des.* **2014**, *14*, 6357–6366.
- (36) Sauter, A.; Roosen-Runge, F.; Zhang, F.; Lotze, G.; Jacobs, R. M. J.; Schreiber, F. Real-Time Observation of Nonclassical Protein Crystallization Kinetics. *J. Am. Chem. Soc.* **2015**, *137*, 1485–1491.
- (37) Sauter, A.; Roosen-Runge, F.; Zhang, F.; Lotze, G.; Feoktystov, A.; Jacobs, R. M. J.; Schreiber, F. On the Question of Two-Step Nucleation in Protein Crystallization. *Faraday Discuss.* **2015**, *179*, 41–58.
- (38) Roosen-Runge, F.; Zhang, F.; Schreiber, F.; Roth, R. Ion-activated Attractive Patches as a Mechanism for Controlled Protein Interactions. *Sci. Rep.* **2014**, *4*, 7016.
- (39) Verheul, M.; Pedersen, J. S.; Roefs, S. P. F. M.; de Kruijff, K. G. Association Behavior of Native  $\beta$ -Lactoglobulin. *Biopolymers* **1999**, *49*, 11–20.
- (40) Elofsson, U. M.; Paulsson, M. A.; Arnebrant, T. Adsorption of  $\beta$ -Lactoglobulin A and B in Relation to Self-Association: Effect of Concentration and pH. *Langmuir* **1997**, *13*, 1695–1700.
- (41) Sober, H. A. *CRC Handbook of Biochemistry: Selected Data for Molecular Biology*; The Chemical Rubber Co.: Cleveland, OH, 1970.
- (42) Narayanan, T. In *Soft Matter Characterization*; Borsali, R., R., Pecora, Ed.; Springer: New York, 2008; Chapter 17: Synchrotron Small-Angle X-Ray Scattering.
- (43) Ianeselli, L.; Zhang, F.; Skoda, M. W. A.; Jacobs, R. M. J.; Martin, R. A.; Callow, S.; Prévost, S.; Schreiber, F. Protein–Protein Interactions in Ovalbumin Solutions Studied by Small-Angle

Scattering: Effect of Ionic Strength and the Chemical Nature of Cations. *J. Phys. Chem. B* **2010**, *114*, 3776–3783.

(44) Pipich, V. QtiKWS: User-Friendly Program for Reduction, Visualization, Analysis and Fit of SA(N)S Data. <http://www.qtikws.de>, 2012.

(45) Zhang, F.; Skoda, M.W. A.; Jacobs, R. M. J.; Martin, R. A.; Martin, C. M.; Schreiber, F. Protein Interactions Studied by SAXS: Effect of Ionic Strength and Protein Concentration for BSA in Aqueous Solutions. *J. Phys. Chem. B* **2007**, *111*, 251–259.

(46) Kline, S. R. Reduction and Analysis of SANS and USANS Data Using IGOR Pro. *J. Appl. Crystallogr.* **2006**, *39*, 895–900.

(47) Ashcroft, N.; Lekner, J. Structure and Resistivity of Liquid Metals. *Phys. Rev.* **1966**, *145*, 83–90.

(48) Sharma, R. V.; Sharma, K. C. The Structure Factor and the Transport Properties of Dense Fluids Having Molecules with Square Well Potential, a Possible Generalization. *Phys. A* **1977**, *89*, 213–218.

(49) Hayter, J. B.; Penfold, J. An Analytic Structure Factor for Macroion Solutions. *Mol. Phys.* **1981**, *42*, 109–118.

(50) Hansen, J.-P.; Hayter, J. B. A Rescaled MSA Structure Factor for Dilute Charged Colloidal Dispersions. *Mol. Phys.* **1982**, *46*, 651–656.

(51) Zhang, F.; Roosen-Runge, F.; Sauter, A.; Roth, R.; Skoda, M. W. A.; Jacobs, R.; Sztucki, M.; Schreiber, F. The Role of Cluster Formation and Metastable Liquid-Liquid Phase Separation in Protein Crystallization. *Faraday Discuss.* **2012**, *159*, 313–325.

(52) Schmitt, C.; Moitzi, C.; Bovay, C.; Rouvet, M.; Bovetto, L.; Donato, L.; Leser, M. E.; Schurtenberger, P.; Stradner, A. Internal Structure and Colloidal Behaviour of Covalent Whey Protein Microgels Obtained by Heat Treatment. *Soft Matter* **2010**, *6*, 4876–4884.

(53) Moitzi, C.; Donato, L.; Schmitt, C.; Bovetto, L.; Gillies, G.; Stradner, A. Structure of  $\beta$ -Lactoglobulin Microgels Formed During Heating as Revealed by Small-Angle X-Ray Scattering and Light Scattering. *Food Hydrocolloids* **2011**, *25*, 1766–1774.

(54) Zhang, F.; Roosen-Runge, F.; Skoda, M. W. A.; Jacobs, R. M. J.; Wolf, M.; Callow, P.; Frielinghaus, H.; Pipich, V.; Prevost, S.; Schreiber, F. Hydration and Interactions in Protein Solutions Containing Concentrated Electrolytes Studied by Small-Angle Scattering. *Phys. Chem. Chem. Phys.* **2012**, *14*, 2483–2493.

(55) Nicolai, T.; Pouzot, M.; Durand, D.; Weijers, M.; Visschers, R. W. Iso-Scattering Points during Heat-Induced Aggregation and Gelation of Globular Proteins Indicating Micro-Phase Separation. *Europhysics Letters (EPL)* **2006**, *73*, 299–305.